Conductivity−Viscosity−Structure: Unpicking the Relationship in an Ionic Liquid[†]

Mathieu Salanne, Christian Simon, and Pierre Turq

Université Pierre et Marie Curie-Paris6, CNRS, ESPCI, UMR 7612, laboratoire LI2C, case courrier 51, 4 Place Jussieu, 75252 Paris Cedex 05, France

Paul A. Madden*

School of Chemistry, University of Edinburgh, Edinburgh EH9 3JJ, U.K.

Received: October 27, 2006; In Final Form: January 19, 2007

The relationships between the ionic mobility, the viscosity, and the atomic-scale structure are investigated in computer simulations of mixtures of LiF and the network glass-forming material BeF_2. The simulations span a wide range of compositions, across which the fluidity of the system changes greatly due to the break-up of the Be−F network by the addition of the LiF. The relationship between the conductivity and viscosity passes from that expected for independently diffusing ions in the dilute mixtures to strongly decoupled Li^+ migration through a viscous network at higher concentrations. The transition between these régimes is linked to the changing local and intermediate-scale structure in the melts. The decoupling phenomenon is associated with the appearance of migration channels in the network which leads to cooperative effects in the Li^+ migration.

I. Introduction

A universal property of *all* ionic liquids is that they conduct electricity by ionic diffusion. A persistent theme of research, motivated in part by the desire to make amorphous electrolytes, has been to understand the relationship between the conductivity and the underlying intermolecular interactions as reflected in the microscopic structure of the fluid or at a more empirical level to the viscosity.[1] The development of a first-principles-based simulation model for LiF−BeF_2 mixtures,[2] which *accurately* reproduces the properties of the real liquid,[3] presents an opportunity to examine this triangular relationship with unprecedented detail across the range from a highly mobile fluid to a highly viscous state.

BeF_2 is a structural analogue of SiO_2, forming the same crystalline polymorphs[4] and exhibiting a similar "strong" glass transition characteristic of a network-forming system. Mixing it with LiF has a similar effect on the fluidity to that of Na_2O on SiO_2; the network is progressively broken down with a consequential reduction in the viscosity until at low BeF_2 concentrations it becomes a simple dissociated melt, best considered as a mixture of Li^+, F^-, and BeF_4^{2-}, as we shall see. Compared to the analogous Na_2O−SiO_2 system, a major advantage for liquid state studies of LiF−BeF_2 is that its glass transition temperature is much lower (592 K for pure BeF_2, compared to 1448 K for pure SiO_2), making microscopic experiments on the liquid state possible. Mixtures of LiF with BeF_2 ("FLiBe") were used as a solvent and as a heat exchanger in the experimental molten salt fission reactors of Oak Ridge in the 1970s. New versions of the molten salt reactor using FLiBe are under development,[5] and it is also a candidate material to be used as a blanket in fusion-breeder reactors.[6] Because of these potential applications, an enormous amount of experimental work has been done on FLiBe, and it is by far the best-characterized fluoride melt. Structural data were obtained from X-ray diffraction experiments[7] and from Raman spectroscopy;[8,9]

the latter showed evidence for the formation of fluoroberyllate species, $Be_nF_{3n+1}^{(n+1)-}$, in the mixtures; these may be considered as fragments of the original BeF_2 network. Dynamical properties like the conductivities[10] and the viscosities[11] have also been measured, and their dependence on the melt composition has been linked to the development of the network.[12]

In our previous study, we were concerned with demonstrating the ability of the interaction potential to reproduce the measured quantities, and thus, our chosen temperature range was as close as possible to that in which experiments had been done (for some compositions at low temperatures, FLiBe becomes so viscous that it cannot be equilibrated in molecular dynamics (MD) simulations of reasonable length). In this work, we will follow the behavior of the conductivity, diffusion, and viscosity (and various microscopic measures of structure and dynamics) across an isotherm at 1200 K which allows examination of a range of compositions where, as we shall see, the fluidity and degree of network formation span a wide range. At low concentrations of BeF_2 in LiF, the mixture behaves as a well-dissociated ionic melt consisting of Li^+, BeF_4^{2-}, and F^- ions, but as the BeF_2 concentration increases, a network forms, resulting in a large increase in viscosity, but with the remaining Li^+ ions relatively free to diffuse within it, so that a "decoupling" between the conductivity and viscosity occurs. It is this process which we wish to trace at the atomistic level. By working at constant temperature, we expect the rates of elementary dynamical steps to be constant (such as the breaking of a bond in an isolated molecule for which we might anticipate a constant activation energy). This allows us to set a "clock" with which to judge the relative rates of different processes. Because of the interest in glassy Li^+ conductors, we have also performed some simulations on deeply cooled samples at high BeF_2 concentration. These calculations were performed to allow us to examine how the decoupling phenomenon persisted into the glassy domain.

We studied nine different FLiBe compositions, ranging from 9.1 to 80% in BeF_2 at 1200 K. At this temperature, we can

---

[†] Part of the special issue "Physical Chemistry of Ionic Liquids".

Conductivity−Viscosity−Structure Relationship

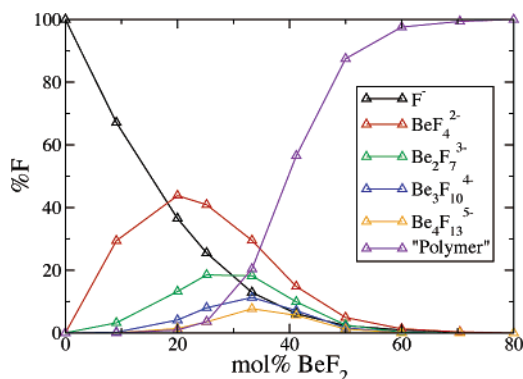*J. Phys. Chem. B, Vol. 111, No. 18, 2007* **4679**

Figure 1. Percentage of F atoms involved in various species observed in the system as a function of composition; "polymer" means a cluster with a Be nuclearity greater than 4, whereas F^- implies that the ion is coordinated only to Li^+.

comfortably equilibrate fluids even at the BeF_2-rich end of this composition range in simulations of about 1 ns duration; more concentrated melts cannot be equilibrated below 1300 K.[2] We also conducted a series of calculations in which the 80% BeF_2 mixture was cooled to 1000 and 800 K. The simulation cells contained 288 F^- ions (and the corresponding number of Li^+ and Be^{2+} ions), and their sizes were equilibrated in NPT runs to reach a pressure of zero; we discussed the good reproduction of the equation of state in the previous work. Long simulations were then performed to gather statistics in the NVT ensemble through the use of a Nosé−Hoover thermostat. Other details of the calculations, including a description of the interaction potentials, are the same as those in refs 2 and 3.

II. Structure ("Speciation") And The Viscosity

In the very dilute solutions of BeF_2 in LiF, the structure is best considered as comprising a mixture of Li^+, F^-, and BeF_4^{2-} units. As described in ref 3, the radial correlation functions show a tight shell of exactly four F^- ions around each Be^{2+} with a deep minimum between the first peak in g_{BeF} and the bulk. Furthermore, the lifetime of a given Be−F "bond" (≈ 7 ps at 1200 K; see below), obtained from the cage correlation time[3,13] for the BeF_4^{2-} ion, is much longer than the structural relaxation time of the dilute solutions. Consequently, in this régime, the BeF_4^{2-} units remain intact while the fluid completes its relaxation to an imposed shear. Experimentally, the species is sufficiently long-lived to give discrete Raman bands[3,8,9] in a spectrum which matches that expected for tetrahedral symmetry.

As the concentration of BeF_2 is increased, more complex species based upon linkages between BeF_4^{2-} units form. These are identified by finding pairs of Be^{2+} ions which have common F^- ions in their coordination shells. We may follow the formation of more complex species by identifying a pair of Be^{2+} ions sharing a common F^- as a link in a molecule and then finding the other Be^{2+} ions to which these are linked in turn, and continuing until we find the ends of the molecule (no further links). First, $Be_2F_7^{3-}$ appears, comprising two BeF_4^{2-} units sharing a common F^- ion, followed by $Be_3F_{10}^{4-}$, and so forth. In our simulations, we see only corner-sharing of the coordination polyhedra, that is, sharing of a single F^- by a given pair of Be^{2+} ions. This exercise enables us to characterize the speciation of the melt as the composition is varied, and the results are illustrated in Figure 1 which shows the fraction of the Be^{2+} ions which are involved in a species with n links. Up to a concentration of about 33% BeF_2 (the Li_2BeF_4 composition normally referred to as FLiBe in the nuclear technologies), the melt primarily contains isolated BeF_4^{2-} and $Be_2F_7^{3-}$ units;

beyond this, we see a rapid increase in the length of the BeF_2-containing species as the concentration is increased. A "polymer" in this figure is a species with more than four internal links. By the highest concentrations, we see that all of the Be^{2+} ions are involved in an extended network which fills the simulation cell.

The influence of this speciation on the properties of the mixtures has been the subject of much interest, notably in the work of Baes.[12] In our previous work, which covered a relatively small range of compositions at lower temperatures, we showed that the viscosity of the system was closely related to its polymerization state.[3] The shear viscosity is obtained from the time integral of the correlation function of the off-diagonal elements of the stress tensor ($\sigma_{\alpha b}$) and requires very long runs in viscous systems:

$$\eta(t) = \frac{\beta}{V} \int_0^t \langle \sigma_{xy}(t') \, \sigma_{xy}(0) \rangle \, dt' \tag{1}$$

The viscosity (strictly the limit as $t \rightarrow \infty$) is then given by the plateau value of the running integral. We adjusted our simulation run length for the different compositions in order to ensure that the stress tensor integral reached a well-defined plateau with good statistics (such that the fluctuations of the running integral about the plateau value gave a standard deviation of about 2% in the estimated viscosity value); this required runs of ~ 5 ns length for the most concentrated solution, where the calculated viscosity is 40 cP at 1200 K. In order to look more closely at the relationship between viscosity and degree of polymerization, we calculated the structural relaxation time (or Maxwell time, $\tau_{Maxwell}$) for all of the studied compositions. In a phenomenological description, the viscosity is written as the product of a shear modulus (the resistance to strain in the absence of relaxation) and the structural relaxation time, and the shear modulus shows only weak compositional and temperature dependence, so that the increase in viscosity is associated with an increase in the Maxwell time. We obtain values for $\tau_{Maxwell}$ from the time for which $\eta(\tau_{Maxwell})/\eta(t \rightarrow \infty) = 1 - (1/e)$.

We compared $\tau_{Maxwell}$ to various microscopic relaxation times of the system, obtained from cage correlation functions, calculated as described in ref 3. The objective is to try to see what kind of microscopic event is dominating the structural relaxation, as sensed by the relaxation time of the stress tensor, at different melt compositions. The first solvation shell breaking times for Li^+ and Be^{2+} are obtained from the Li−F and Be−F cage correlation functions, and respectively denoted τ_{LiF} and τ_{BeF}. We also considered the Be−F−Be bond breaking time, which was obtained from the Be−Be cage correlation function; this we will regard as a relaxation time of the network ($\tau_{network}$), since reorganization of the network will involve the breaking of internal Be−Be bonds. In Figure 2, we represent the composition dependence of these various times (top left-hand panel) and also plot the variation of $\tau_{Maxwell}$ against the other characteristic times (in the remaining panels of the figure). There appear to be two limiting régimes in the relationship of these times, at very low and very high BeF_2 concentration, together with an intermediate region over which the network formation is developing (Figure 1).

The region of "low" BeF_2 concentrations is below about 33% BeF_2 (which corresponds to the fourth point from the left appearing in the figures) where, as we have seen, the melt is well dissociated. Here, $\tau_{Maxwell}$ is close to τ_{LiF} and we interpret the structural relaxation to correspond to the Li^+ first shell reorganization. τ_{BeF} is much longer than $\tau_{Maxwell}$ in this régime, showing that the BeF_4^{2-} units remain intact on the time scale
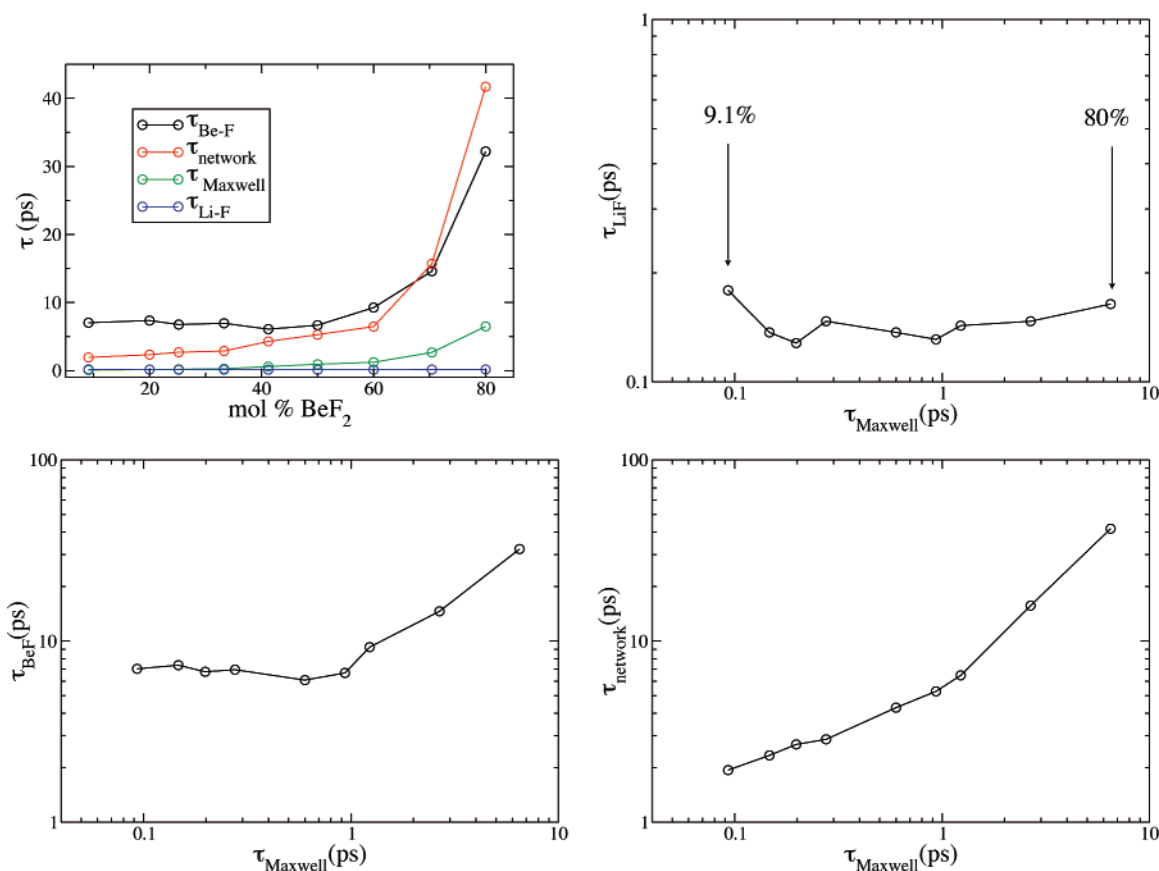
Figure 2. The upper left-hand panel shows a plot of the various relaxation times—$\tau_{network}$, $\tau_{Maxwell}$, τ_{LiF}, and τ_{BeF}—versus BeF$_2$ concentration. The remaining panels show the relationship between the various microscopic times and $\tau_{Maxwell}$: in these latter panels, the points correspond to the sequence of concentrations evident from the first panel, with the lowest concentration point at the left.

of the structural relaxation and their internal reorganizations do not contribute to the relaxation of an applied strain—they behave as rigid bodies. Both τ_{LiF} and τ_{BeF} are almost concentration independent across this concentration domain, indicating that the breaking of the "bonds" which hold the coordination complexes together can be considered as a simple unimolecular process. The viscosity (and $\tau_{Maxwell}$) are slowly increasing as the BeF$_2$ concentration is increasing because the fluid contains an increasing number of the larger, rigid BeF$_4{}^{2-}$ units, that is, for the same reason that the viscosity of a dilute colloidal suspension increases with the concentration of colloidal particles. In this low concentration region, $\tau_{network}$ would not be expected to play a significant role, as the concentration of Be−F−Be bonds in species like Be$_2$F$_7{}^{3-}$ is not large enough to influence the viscosity (see Figure 1).

At high concentration, beyond about 50% BeF$_2$, Figure 1 indicates the progressive growth of an all-pervading network and $\tau_{Maxwell}$ increases sharply with increasing BeF$_2$ concentration. This increase is not reflected in τ_{LiF} which remains almost constant, as shown in the upper right-hand panel of Figure 2, indicating that the elementary events of breaking bonds in the first Li$^+$ coordination shells continue to behave as simple activated process with constant rates along the isotherm and independently of the state of association of the melt. $\tau_{Maxwell}$ is much longer than τ_{LiF}, showing that the structural relaxation now involves some slower process. Instead, we find (final panel of Figure 2) that $\tau_{Maxwell}$ is proportional to $\tau_{network}$, indicating that network relaxation now dominates the response to a shear. Our network relaxation time is based upon the breaking rate of a single Be−Be bond, but the network can relax by the breaking of many of its internal connections, so we would expect $\tau_{network}$ to exceed $\tau_{Maxwell}$ in the way indicated. It is, at first sight,

surprising to see that the breaking time of Be−Be and Be−F bonds should show such a rapid increase with BeF$_2$ concentration beyond 50%, whereas the Li−F breaking time is composition independent. It appears that the altered behavior at higher BeF$_2$ concentrations arises because the Be−Be separation is trapped by the surrounding network so that the two Be ions are not able to move apart and the bonds between them cannot break. Any Be−F linkage is held in place not just by the direct bond but also by a more complex path of bonds involving several other Be^{2+} and F$^-$ ions. It appears that the cooperativity of the network relaxation is expressed even at this local level: the increase in the structural relaxation time of the whole fluid is not simply due to the presence of a network of increasing size but is also due to the fact that the network itself is relaxing on progressively longer time scales.

III. Diffusion/Conductivity and the Viscosity

A. Breakdown of Stokes' Law. It is normal to examine the relationship between viscosity (η) and diffusion coefficient (D) in the form suggested by Stokes' law

$$\eta D = \frac{k_B T}{n \pi a} \tag{2}$$

where a is a length ("hydrodynamic radius") characteristic of the size of the diffusing object and n takes the value 4 for a smooth spherical object (slip-boundary condition) and 6 for a rough one (stick). We show results for the product ηD for the Li$^+$ and Be^{2+} ions in Figure 3. The diffusion coefficients in this figure were obtained from the slope of the mean-squared displacement of the ions versus time, taken at times sufficiently
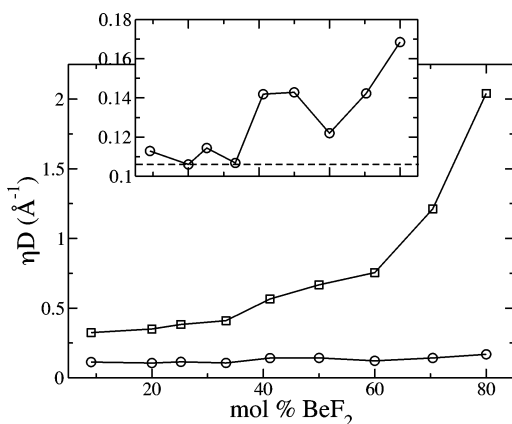
Conductivity−Viscosity−Structure Relationship

J. Phys. Chem. B, Vol. 111, No. 18, 2007 **4681**

Figure 3. Product of the viscosity and of the diffusion coefficient for the two cations (squares, Li$^+$; circle, Be^{2+}). The inset shows an enlargement of the Be^{2+} curve, and the horizontal dashed line is the predicted value for the product when we use the first peak in the Be−F radial distribution function as an estimate of the size of the BeF$_4^{2-}$ ion.

long that the ions had diffused much further than their characteristic distance from a nearest F$^-$ ion.

For the well-dissociated melt, as exemplified by the dilute mixtures, we expect the value of the product to be a constant for each ion. Furthermore, given the long lifetime of the BeF$_4^{2-}$ ion relative to the structural relaxation time, we expect[14] the values of these constants to be close to those calculated with a_{Li^+} given by the crystallographic radius of Li$^+$ and by the size of the BeF$_4^{2-}$ ion for Be^{2+}, respectively. The horizontal dashed line in the inset to the figure shows these estimates of the product for Be^{2+}, where we have used the position of the first peak in g_{BeF} as an estimate of the radius of BeF$_4^{2-}$ and the stick boundary condition. It can be seen that the Stokes' law expectation of a roughly constant value for the product ηD is reasonably well borne out by the data for the Be^{2+} ions, and also for Li$^+$ at the lowest concentrations, but this is definitely not the case for Li$^+$ at high BeF$_2$ concentrations.

In fact, for the more concentrated mixtures, we see dramatic departures from the Stokes' law expectation for the Li$^+$ ion, where the diffusion progressively increases above the expected value and by a substantial amount at the highest concentrations. This reflects *decoupling* of the Li$^+$ diffusion from the microscopic processes which allow stress relaxation as the fluid becomes more concentrated in BeF$_2$ and the extent of the network formation increases. It is a phenomenon which is of great technological interest,[1] as it is associated with the formation of good ionic conductors in nearly rigid materials with high viscosities, suitable for use in devices. In the analogous alkali silicates, in the glassy state where the Si−O network has become rigid, the alkali cations are known to diffuse through pores or channels in the network. Angell et al.[15] hypothesized that this model could also be applied to alkali cation diffusion in viscous liquids. It appears that a similar effect might explain the enhanced diffusion of the Li$^+$ ions in the concentrated FLiBe mixtures, and with this in mind, we will examine in more detail the behavior of the Li$^+$ diffusion as the melt is more deeply cooled below.

Concerning the Be^{2+} ions, the inset of Figure 3 shows that the product ηD is well approximated by the choice of the BeF$_4^{2-}$ ion radius for diluted systems. This is because, at small concentrations, Be^{2+} diffuses inside BeF$_4^{2-}$ units which remain intact on the time scale of the structural relaxation, as we have seen from the above comparison of τ_{BeF} and $\tau_{Maxwell}$ in this
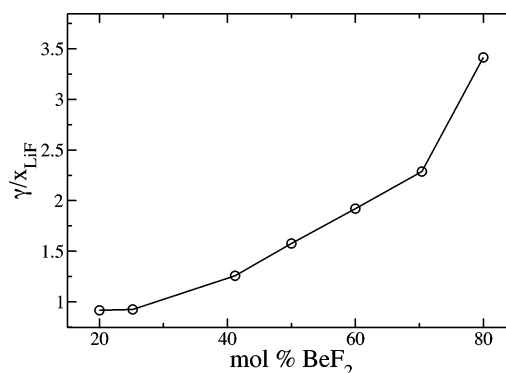

Figure 4. Contribution of the Li$^+$ ions to the total conductivity.

concentration domain. The same kind of result was obtained for the diffusion of trivalent ions in the LiCl−KCl mixture.[14]

B. Conductivity and Diffusion Coefficient: Cooperativity. Although the viscosity dependence of the diffusion process dominates the composition dependence of the conductivity, the relationship between the conductivity and diffusion coefficient is not trivial.

We computed the conductivity of the mixtures from the slope of the mean-squared displacement of the charge density versus time

$$\lambda^K = \frac{\beta e^2}{V} \lim_{t \to \infty} \frac{1}{6t} \langle |\sum_i q^i \delta \mathbf{r}_i(t)|^2 \rangle \tag{3}$$

where $\delta \mathbf{r}_i(t)$ is the displacement of ion i in time t, q^i is the ionic charge, and the sum runs over all ions in the system. Because of the length of the runs, required to get good values for the viscosity, the statistical fluctuations in the mean-squared displacement versus time were small with the deviations from linearity of order 1% over several structural relaxation times. We showed excellent agreement between calculated and measured conductivities in the previous paper[3] and also discussed the relationship between the total conductivity (λ^K) and that calculated from the Nernst−Einstein conductivity, calculated on the assumption of independent diffusion of the ions. Here, we are interested in the degree to which the Li$^+$ ion mobility dominates the conductivity of the system. At low concentrations, the F$^-$ and BeF$_4^{2-}$ ions will also contribute to the conductivity, but as they become tightly coupled together in the network, we expect the total conductivity to become increasingly close to the value calculated for the Li$^+$ ions alone.[3] The lithium ion contribution (λ_{Li}^K), is obtained from the mean displacement of all of the Li$^+$ ions together in the simulation box:

$$\lambda_{Li}^K = \frac{\beta e^2}{V} \lim_{t \to \infty} \frac{1}{6t} \langle |\Delta_{Li}(t)|^2 \rangle \tag{4}$$

where $\Delta_{Li}(t) = \sum_{i \in N_{Li}} \delta \mathbf{r}_i(t)$ is the displacement of all of the Li$^+$ ions at time t.

In Figure 4, we show the quantity γ, given by

$$\gamma = \frac{\lambda_{Li}^K}{\lambda^K} \tag{5}$$

divided by the LiF mole fraction as a measure of the extent to which each lithium ion contributes to the calculated conductivity. As the BeF$_2$ concentration increases, we see that the lithium ions dominate the conductivity to a progressively increasing extent, indicating that the picture of mobile Li$^+$ ions loosely bound to a very slowly relaxing network of BeF$_4^{2-}$ units is valid.
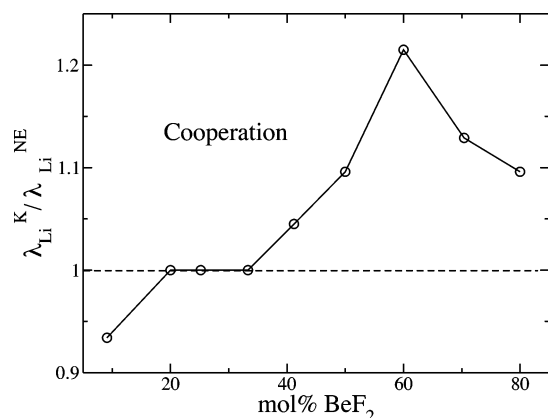
Figure 5. Illustration of the cooperativity of the Li^+ ions in the BeF_2-rich region.

The lithium ion conductivity (λ_{Li}^K) is different from that estimated from the Nernst–Einstein equation (λ_{Li}^{NE}), in which all of the Li^+ ions are presumed to be moving independently:

$$\lambda_{Li}^{NE} = \frac{\beta e^2 N_{Li}}{V} \lim_{t \to \infty} \frac{1}{6t} \langle |\delta \mathbf{r}_i(t)|^2 \rangle \qquad (6)$$

Comparison of λ_{Li}^K and λ_{Li}^{NE} provides a macroscopic measure on the importance of *cooperative* effects in the lithium ion diffusion. If there is no correlation between the Li^+ ion motions, then we will have $\lambda_{Li}^K = \lambda_{Li}^{NE}$. If there is a cooperative motion of the ions in which the Li^+ ions tend to displace themselves in the same direction, then λ_{Li}^K will be greater than λ_{Li}^{NE}; if they displace in opposite directions, $\lambda_{Li}^K < \lambda_{Li}^{NE}$. Although the deviation from unity is small, we regard the results as reliable in view of the high statistical accuracy of the calculated conductivities because of the length of the simulation runs. We can see from Figure 5, where $\lambda_{Li}^K / \lambda_{Li}^{NE}$ versus the composition of the system is displayed, that a cooperative régime appears for $x_{BeF_2} > 0.33$, that is, when the fluoroberyllate networks start to appear. This result is consistent with the hypothesis mentioned above, of the emergence of ionic conduction channels in a relatively slowly relaxing network, an idea we will explore further below. In the work of Lammert et al.[17,18] on alkali silicate *glasses*, the conduction channels consist of strings of sites which loosely bind an alkali cation to the network and which are sufficiently close to allow intersite hopping to occur. They found that most of these sites were occupied and suggested that diffusion occurred via a vacancy mechanism, which would impart a cooperative quality to the ionic motion. A particular feature of our Figure 5 is the existence of a composition (x_{BeF_2} = 0.60) for which the cooperativity is maximal. As we shall see, there is structural evidence of significant correlations between the positions of the Li ions in the same composition range.

C. Medium-Range Ordering of Li^+ Ions. The idea of ionic conduction channels provides an appealing picture to account for the decoupling of the Li^+ diffusion from the viscosity and for some cooperativity in the collective diffusion, but it is difficult to substantiate directly in the melt at 1200 K because the relaxation time of the network, and hence the channels, is not much greater than the time scale for diffusion of the Li^+ ions themselves. We will examine the supercooled domain in the next section, but before doing so, we point to one other piece of evidence from the simulations at high temperature to support the idea that the spatial arrangement of the Li^+ ions becomes controlled by the presence of the network in the BeF_2-rich composition domain.

Li–Li and Be–Be partial structure factors, for example,

$$S_{LiLi}(k) = \left\langle N_{Li}^{-1} \sum_{i,j} e^{i\mathbf{k} \cdot \mathbf{r}_{ij}} \right\rangle \qquad (7)$$

where the sum runs over all N_{Li} lithium ions in the sample, calculated across the composition range, are compared in Figure 6. We are particularly interested in the emergence of a so-called prepeak in the Li–Li structure factors in the region of $k \sim 1.5$ Å^{-1}, which is indicative of intermediate-range order. At low BeF_2 concentrations, in the well-dissociated melt, S_{LiLi} is dominated by the principal peak at $k \sim 2.5$ Å^{-1} which is associated with the normal nearest neighbor separation of the Li^+ ions in molten LiF (which occurs on the length scale of the Li–F–Li configuration). In the same concentration range, the Be^{2+} ions are tied up in the fluoroberyllate units which, as larger and more highly charged units, are more widely separated and responsible for the prominent peak at $k \sim 1.5$ Å^{-1} which dominates S_{BeBe} at these concentrations (i.e., this could be regarded as the principal peak for a "spherical" fluoroberyllate ion in a fully dissociated melt, in the same manner as that used to describe the contribution of Zn–Zn correlations to the prepeak in $RbCl$–$ZnCl_2$ mixtures[22]). At intermediate BeF_2 concentrations, as we have seen, the network begins to form (this has already begun to happen at the lowest concentration illustrated in the figure—25%) and a peak appears at higher k in S_{BeBe}, $k \sim 2.7$ Å^{-1}, which is due to the emergence of Be–F–Be configurations. The lower k peak persists, however, and can be associated with the correlations between Be ions which are not directly bonded in the network; such low k features are very characteristic of tetrahedrally coordinated networks.[19–21] In this intermediate concentration range (33–60% BeF_2), we see the appearance of a broad prepeak in S_{LiLi} at similar k values to that in S_{BeBe}. This indicates that the correlations between the lithium ions is being set by the way that they arrange themselves around the BeF_2 network. Finally, at the highest BeF_2 concentrations, there are so few Li^+ ions in the sample that there are effectively no correlations between them and the structure factor becomes virtually flat. (Note, however, that there is some suggestion of a rise in the structure factor toward low k which is suggestive of a phase separation.)

Meyer et al. have shown the emergence of similar prepeaks in the Na–Na partial structure factor in sodium silicate glass.[23] They observed the same feature in the experimental neutron diffraction pattern and in computer simulations. From the latter, they showed that the intermediate-range order associated with the prepeak was a signature of the concentration of sodium ions into pores within the silicate network structure and suggested that this provided an observable structural signature of the diffusion channels believed to exist in these glasses. In our calculations, we note that the concentration régime in which the prepeak forms in S_{LiLi} is that in which we demonstrated cooperative diffusion in the previous section.

IV. Diffusion in The Deeply Cooled Fluid

As has been indicated above, as the concentration of BeF_2 in the mixtures exceeds about 33%, the Li^+ diffusion decouples from the viscosity which itself increases rapidly with the BeF_2 concentration due to the formation of a Be–F network. In Angell's analysis,[1] these properties of the melt suggest that a glassy BeF_2–LiF mixture would be a good candidate for an amorphous solid lithium ion conductor. We have already pointed to some similarities between the properties of the melt and those of Na_2O–SiO_2 glassy mixtures, which are well-known ionic
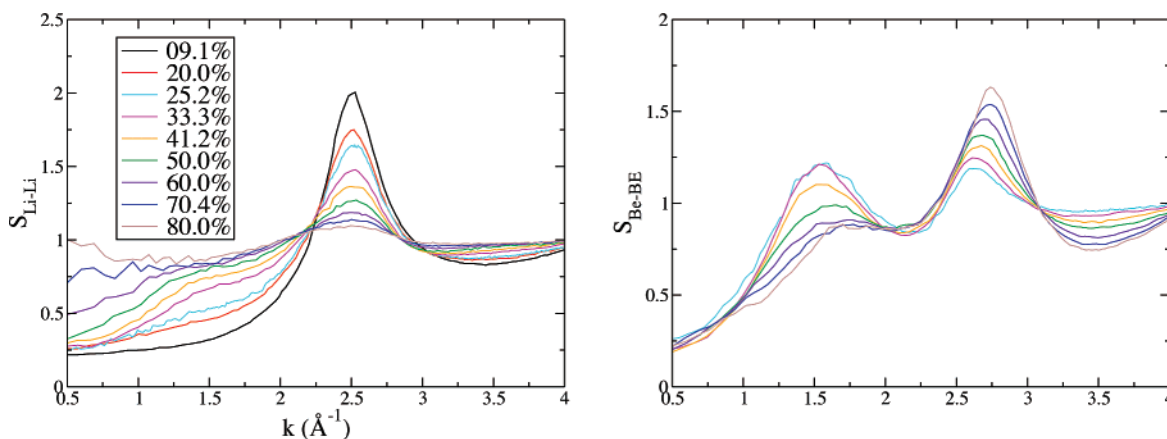
Conductivity−Viscosity−Structure Relationship

J. Phys. Chem. B, Vol. 111, No. 18, 2007 **4683**

Figure 6. Li−Li partial structure factor and Be−Be partial structure factors for melts of different composition. The peaks at ∼2.5 and ∼2.7 Å^{-1} in the two structure factors are referred to in the text as the principal peaks and those at ∼1.5 Å^{-1} as the prepeaks.
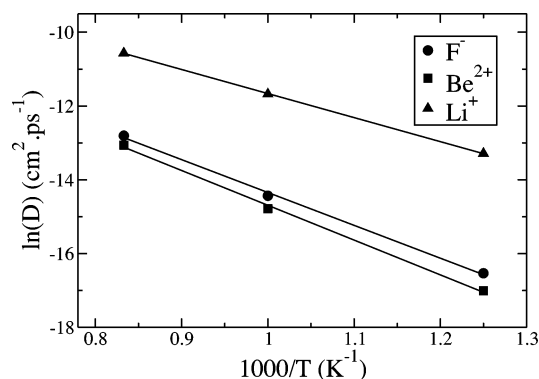

Figure 7. Diffusion coefficients of Li$^+$, Be^{2+}, and F$^-$ ions in deeply cooled samples of the mixtures with 80% BeF$_2$ presented as an Arrhenius plot.

conductors. To pursue these ideas further, we prepared deeply cooled samples from the 80% BeF$_2$ mixtures at 1200 K by rapidly reducing the temperature to 1000 and 800 K and then conducting long simulations of several million MD steps, corresponding to several nanoseconds of real time. Notice that even runs of this length are not sufficient to fully equilibrate these deeply cooled fluids or to calculate collective quantities like their viscosities.

In Figure 7, we show the diffusion coefficients of the three species in the form of an Arrhenius plot. We see that the diffusion coefficients of Be^{2+} and F$^-$ ions are equal, consistent with them being bound together in a network. They are already substantially smaller than that of the Li$^+$ ion at 1200 K and decrease more rapidly with decreasing temperature; an activation energy of 76 kJ mol^{-1} is found for the Be^{2+} and F$^-$ ions compared to 54 kJ mol^{-1} for Li$^+$. It does therefore seem that the decoupling phenomenon persists to lower temperatures and, in fact, becomes even more pronounced, perhaps due to the increasing immobility of the Be−F network.

Because of the increased time-scale separation between the relaxation of the network and the Li$^+$ diffusion at low temperature, it becomes possible to examine directly the idea that the decoupling phenomenon is associated with the appearance of conduction channels within the BeF$_2$ network. Lammert et al.[17,18] have introduced a scheme for characterizing these channels in the sodium silicates, and we have broadly followed their approach in what follows. The simulation cell (of side 18.4 Å) is divided into 50 × 50 × 50 subcells, and the presence or absence of Li$^+$ ions within the cells is monitored at intervals of 100 MD steps (=50 fs) along the simulation trajectory. This sampling therefore occurs on 20 000 occasions during 1 ns of
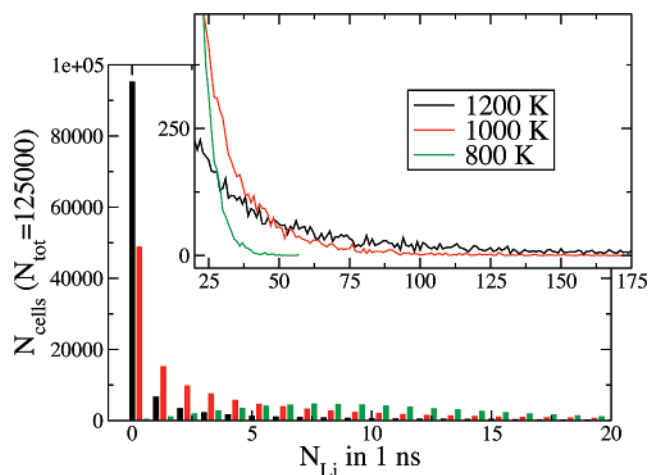

Figure 8. Probability distribution for a cell to be visited by N_{Li} times in 1 ns of simulation. This distribution is showed as histograms in the main figure and as a continuous line in the inset.

the simulation trajectory. Figure 8 shows the probability distribution for a subcell to be occupied for a certain number of these sampling occasions.

At 1200 K, we see that the probability distribution is peaked around 6, which is close to what we would expect for the mean number of visits to any single cell if the 32 Li$^+$ ions in the simulation are distributed across the 125 000 subcells with equal probability over the 20 000 occasions. At lower temperatures, however, we see that the main peak of the distribution is around zero, and the peak becomes sharper as the temperature drops. This implies that there are many subcells which are never visited by any Li$^+$ ion during the trajectory; these are the cells which are blocked by the presence of the Be−F network which is not moving substantially on the time scale of the simulation at these temperatures.

In this low temperature region, we can now visualize the spatial distribution of the subcells which are occupied; we find that they are grouped together to form extended channels in a similar manner to that observed in alkali silicates by Meyer et al.[23] and Lammert et al.[17,18] In the left-hand panel of Figure 9, we have represented the isosurfaces which bound regions of space whose subcells are occupied by Li$^+$ ions on more than 36 occasions in 1 ns, that is, whose occupations exceed by a factor of 6 the value expected for the average occupation if the Li$^+$ ions were able to distribute themselves uniformly through space. The isosurfaces are seen to have the appearance of channels which extend across large regions of the simulation
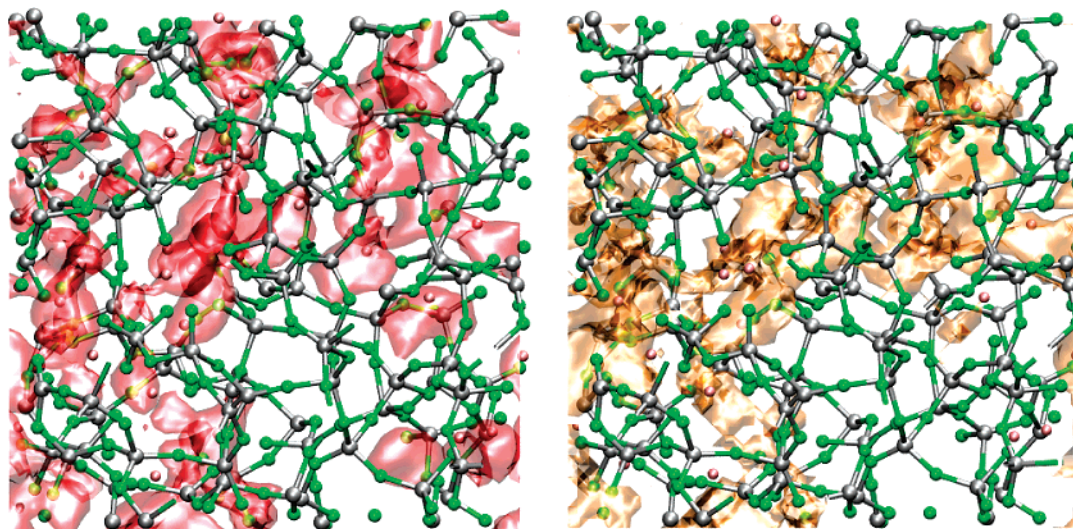
Figure 9. Isosurfaces of the subcells with a high occupancy by Li$^+$ ions at 800 K (left) and of the subcells visited by more than three *different* Li$^+$ ions (right): note the regions bounded by these surface appear to overlap strongly. We have superimposed the ball-and-stick model of the Be−F network from the starting configuration of the simulation.

cell. However, we should note that a subcell could acquire a high occupation by being close to a site about which an *immobile* ion was oscillating. We have therefore refined the search for mobility channels by selecting for subcells which are visited by more than three *different* Li$^+$ ions in each nanosecond. These channels are displayed in the right-hand panel of Figure 9; they overlap the channels of the first figure and have a similar spatial extent.

V. Summary

As the concentration of BeF$_2$ in LiF−BeF$_2$ mixtures is increased, the viscosity shows a very substantial increase which is qualitatively associated with the progressive formation of an extended fluoroberyllate network. We have traced in some detail how this increase is connected to a change in the mechanism of the dominant routes of relaxation of stress. The internal relaxation of small fluoroberyllate fragments (BeF$_4^{2-}$, Be$_2$F$_7^{3-}$, etc.) is too slow to contribute to the stress relaxation in the relatively dilute solutions (<40% BeF$_2$) where an extended network has not formed: they simply contribute to the viscosity as large (relative to Li$^+$ ions) rigid bodies, resulting in a slow increase in the viscosity with increasing concentration. When the network begins to extend through the simulation cell, its internal relaxation takes over as the mechanism of stress tensor relaxation, and the viscosity shows a sharp rise. In the same concentration range, the Li$^+$ ion motion begins to dominate the conductivity and the Li$^+$ diffusion coefficient (and conductivity) exhibit a remarkable decoupling from the viscosity. It has been suggested[15] that this decoupling process can be associated with the formation of Li$^+$ mobility channels within the fluoroberyllate network, by analogy with an established phenomenon in alkali silicate *glasses*. This assignment is difficult to verify directly in the melt, due to the fact that the Li$^+$ diffusion and network relaxation occur on the same time scale, but it is qualitatively consistent with other phenomena, such as the appearance of a prepeak in the Li−Li partial structure factor and an increase in the cooperativity of the Li$^+$ contribution to the conductivity. On deeply cooling the concentrated mixture, we found that the decoupling phenomenon becomes more pronounced. In this highly viscous régime, we were able to substantiate directly the idea that the mobile Li$^+$ ions were concentrated into channels.

References and Notes

(1) Angell, C. A.; Imrie, C. T.; Ingram, M. D. *Polym. Int.* **1998**, *47*, 9.

(2) Heaton, R. J.; Brookes, R.; Madden, P. A.; Salanne, M.; Simon, C.; Turq, P. *J. Phys. Chem. B* **2006**, *110*, 11454.

(3) Salanne, M.; Simon, C.; Turq, P.; Heaton, R. J.; Madden, P. A. *J. Phys. Chem. B* **2006**, *110*, 11461.

(4) Müller, U. *Inorganic Structural Chemistry*; Wiley: Chichester, U.K., 1993.

(5) Forsberg, C. W. *Nucl. Technol.* **2003**, *144*, 289.

(6) Moriyama, H.; Sagara, A.; Tanaka, S.; Moir, R. W.; Sze, D. K. *Fusion Eng. Des.* **1998**, *39*, 627.

(7) Vaslow, F.; Narten, A. H. *J. Chem. Phys.* **1973**, *59*, 4949.

(8) Quist, A. S.; Bates, J. B.; Boyd, G. E. *J. Phys. Chem.* **1972**, *76*, 78.

(9) Toth, L. M.; Bates, J. B.; Boyd, G. E. *J. Phys. Chem.* **1973**, *77*, 216.

(10) Robbins, G. D.; Braunstein, J. *Molten salt reactor program*; Report ORNL-4548; Oak Ridge National Laboratory: Oak Ridge, TN.

(11) Cantor, S.; Ward, W. T.; Moynihan, C. T. *J. Chem. Phys.* **1969**, *50*, 2874.

(12) Baes, C. F., Jr. *J. Solid State Chem.* **1970**, *1*, 159.

(13) Rabani, E.; Gezelter, J. D.; Berne, B. J. *J. Chem. Phys.* **1997**, *107*, 6867.

(14) Brookes, R.; Davies, A.; Ketwaroo, G.; P. A. Madden, P. A. *J. Phys. Chem. B* **2005**, *109*, 6485.

(15) Angell, C. A.; Boehm, L.; Cheeseman, P. A.; Tamaddon, S. *Solid State Ionics* **1981**, *5*, 659.

(16) Hemmati, M.; Moynihan, C. T.; Angell, C. A. *J. Chem. Phys.* **2001**, *115*, 6663.

(17) Lammert, H.; Kunow, M.; Heuer, A. *Phys. Rev. Lett.* **2003**, *90*, 215901.

(18) Lammert, H.; Heuer, A. *Phys. Rev. B* **2004**, *70*, 024204.

(19) Elliott, S. R. *Phys. Rev. Lett.* **1991**, *67*, 711−714.

(20) Salmon, P. S. *Proc. R. Soc. London, Ser. A* **1994**, *425*, 351.

(21) Wilson, M.; Madden, P. A. *Phys. Rev. Lett.* **1998**, *80*, 532.

(22) Wilson, M.; Madden, P. A. *Phys. Rev. Lett.* **1994**, *72*, 3033.

(23) Meyer, A.; Horbach, J.; Kob, W.; Kargl, F.; Schober, H. *Phys. Rev. Lett.* **2004**, *93*, 027801.